

CHEMISTRY

AN ASIAN JOURNAL

www.chemasianj.org

Accepted Article

Title: Enzyme Instructed Self-assembly of Naphthalimide-dipeptide: Spontaneous Transformation from Nanosphere to Nanotubular Structures that Induces Hydrogelation

Authors: Rajan Deepan Chakravarthy, Mohiuddin Mohammed, and Hsin-Chieh Lin

This manuscript has been accepted after peer review and appears as an Accepted Article online prior to editing, proofing, and formal publication of the final Version of Record (VoR). This work is currently citable by using the Digital Object Identifier (DOI) given below. The VoR will be published online in Early View as soon as possible and may be different to this Accepted Article as a result of editing. Readers should obtain the VoR from the journal website shown below when it is published to ensure accuracy of information. The authors are responsible for the content of this Accepted Article.

To be cited as: *Chem. Asian J.* 10.1002/asia.202000575

Link to VoR: <https://doi.org/10.1002/asia.202000575>

A Journal of



A sister journal of *Angewandte Chemie* and *Chemistry – A European Journal*

WILEY-VCH

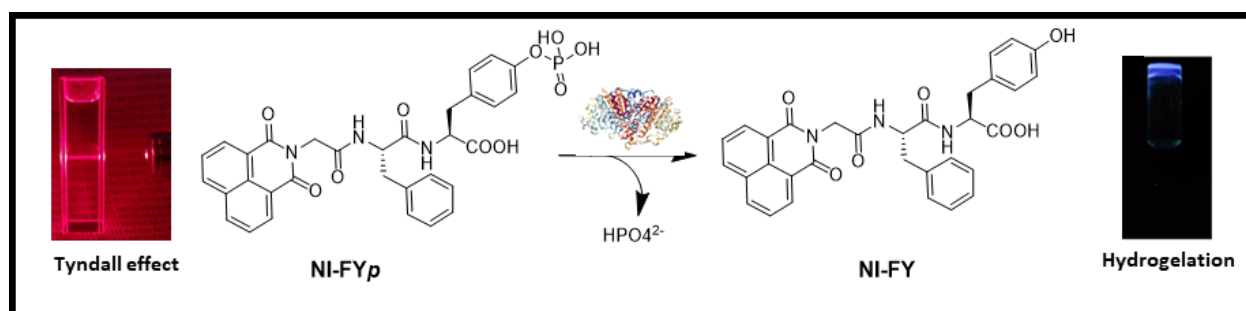
Enzyme Instructed Self-assembly of Naphthalimide-dipeptide: Spontaneous Transformation from Nanosphere to Nanotubular Structures that Induces Hydrogelation

Rajan Deepan Chakravarthy, Mohiuddin Mohammed and Hsin-Chieh Lin*

Department of Materials Science and Engineering, National Chiao Tung University, Hsinchu, Taiwan, Republic of China 300

E-mail: hclin45@nctu.edu.tw

Graphical abstract:



Abstract: Understanding the structure-morphology relationships of the self-assembled nanostructures is very crucial for developing the materials with the desired chemical and biological functions. Here, phosphate-based naphthalimide (NI) derivatives have been developed for the first time to study the enzyme instructed self-assembly process. Self-assembly of simple amino acid derivative **NI-Yp** resulted in non-specific amorphous aggregates in the presence of alkaline phosphatase enzyme. On the other hand, **NI-FYp** dipeptide forms spherical nanoparticles in the aqueous condition which slowly transformed into partially unzipped nanotubular structures during the enzymatic catalytic process through multiple stages which subsequently resulted in hydrogelation. The self-assembly is driven by the formation of β -sheet type structures stabilized by offset aromatic stacking of NI core and hydrogen bonding interactions which is confirmed with PXRD, Congo-red staining and molecular mechanical calculations. We propose a mechanism for the self-assembly process based on TEM and spectroscopic data. The nanotubular structures of **NI-FYp** precursor exhibited higher cytotoxicity to human breast cancer cells and human cervical cancer cells when compared to the nanofiber structures of the similar Fmoc-derivative. Overall this study provides a new understanding of the supramolecular self-assembly of small molecular weight hydrogelators.

Keywords: Supramolecular chemistry • Naphthalimide • Peptide • Enzyme catalysis • Hydrogel

Molecular self-assembly is a critical process in living systems to forming macromolecular assemblies including the construction of lipid bilayers, protein quaternary complex and DNA double helix.^{1,2} In this context, small peptides especially aromatic peptides have particularly been proven to be a versatile class of organic building blocks for self-assembled materials.³⁻⁶ It has been very well established that at the nano-to-mesoscale, the architectures obtained from peptide units exhibit higher stability with a large variety of morphologies, which include nanotubes, nanoribbons, and nanowires.⁷ In addition to that small peptide-based self-assemblies provide significant advantages including biological compatibility, straightforward synthesis and functionalization.⁸ These peptides offer greater flexibility to design and control the supramolecular architectures because of their characteristic self-assembling building blocks and highly stable architecture. The self-assembly of peptide molecules depends on the structural and dynamical properties of their building blocks that are predominantly governed by their amino acid sequences.⁹ The morphologies of these nano-assemblies are crucial for specific applications, e.g., nanoparticles are useful for drug delivery while nanotubes and nanofibers are used for biosensor fabrication and tissue engineering, respectively.¹⁰ Design of peptide-based small molecules to controlling the morphology of self-assembling nanostructures is highly challenging.¹¹⁻²¹ For example, Stupp and coworkers reported the self-assembly of long chain terapeptide amphiphiles that formed a giant nanobelts structures.^{11,12} Ulijn and coworkers have systematically studied the morphological transformations of Fmoc-Yp and Fmoc-FYp materials under enzymatic dephosphorylation method.^{13,14} To our knowledge, there are currently only a few examples of the nanostructure transformation of low molecular

peptide assemblies available. However, recent findings and innovations in the field have created plenty of interest and generous space for further improvements.

Naphthalimide (NI)-derivatives has received increasing attention in recent years due to its unique photophysical property and photostability.^{22,23} Naphthalimides with a variety of functionalization have been investigated as aggregation-induced emission (AIE) luminogens. Recent reviews article summarizes the continuing efforts in this area.²⁴ The significance of NI for various biological applications has also been very well documented.²⁵ More recently NI has been implemented as an aromatic core for creating self-assembled materials due to its strong π -stacking propensity. For example, Tao Yi and coworkers have studied gelation behaviors of NI compounds and they found that materials displayed high fluorescence quantum yields in both solution and solid-state.²⁶ Recently we reported a NI-based supramolecular hydrogelator, which exhibits AIE phenomenon.²⁷⁻²⁹ Particularly, we have shown the self-assembly of NI-F that results in the formation of AIE-active microfibers which facilitate the high contrast visualization of 3D live cell imaging.²⁷ In this work, our focus is to study the self-assembly of phosphate-based NI derivatives.

Enzyme instructed self-assembly (EISA) of small molecules has become an attractive approach in anticancer drug developments, molecular imaging, and nanotechnology.³⁰ Recent studies revealed that EISA-based supramolecular assemblies are not only capable of inhibiting undruggable protein targets of various cancers but also exhibited activities to prevent acquired drug resistance. Hence, EISA is being considered as a reliable complementary anticancer therapy to the ligand-receptor approach.³⁰⁻³² Few attempts have also been made to monitor the EISA process in biological milieu by

conjugating peptides with suitable fluorescent dye molecules.³³ However, the enzymatic hydrogelation with NI based system was never established. NI is an AIE chromophore which is weakly emissive in molecularly dissolved state and highly emissive under self-assembled condition. Integration of such AIE chromophore would be beneficial for selective imaging and killing of tumor cells. In the present work, we develop NI based low molecular weight compounds and examine their self-assembly process under EISA condition. The mechanism of the self-assembly was also systematically investigated using various spectroscopic and microscopic techniques.

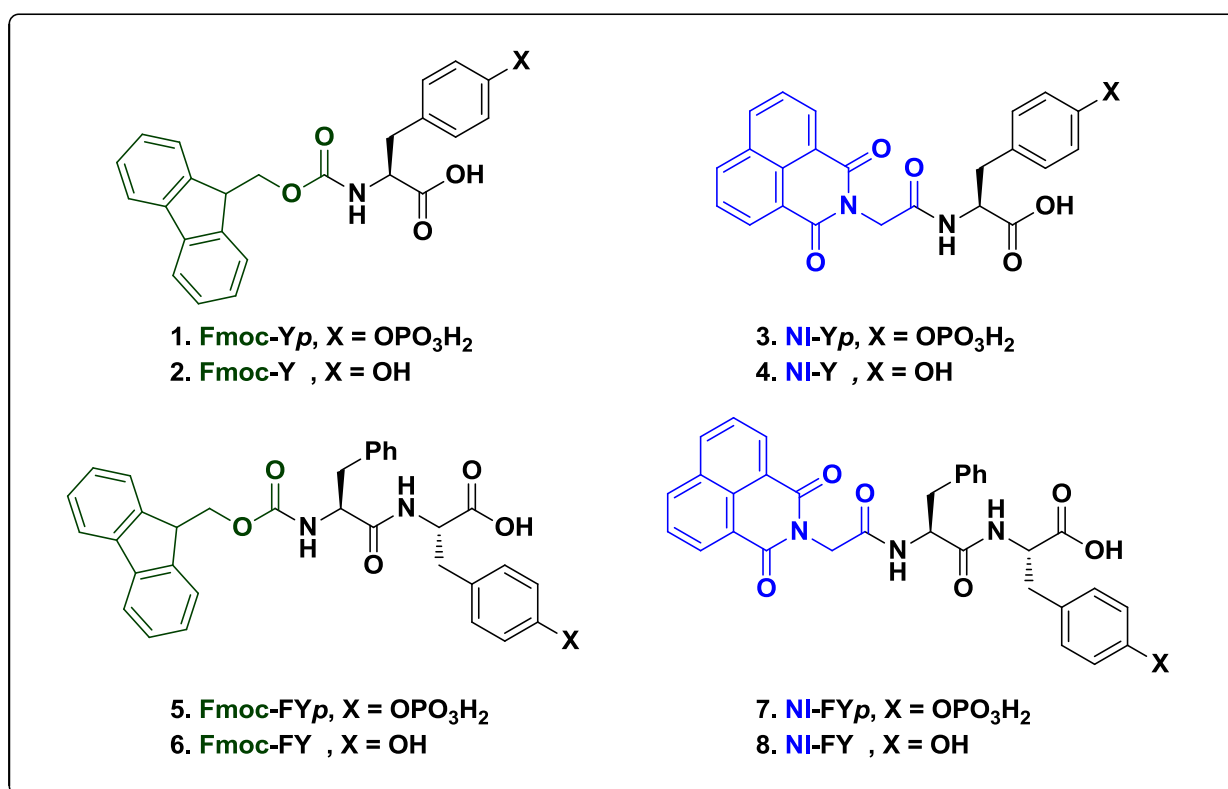


Figure 1. The chemical structures of **Fmoc** and **NI** based compounds used for this study.

Results and Discussion

The supramolecular hydrogelation process of amino acids or short peptide hydrogelators typically requires an aromatic hydrophobic group. NI aromatic unit possess strong hydrophobicity and aromatic π - π stacking system. NI group also having two-dimensional arrangement of p-orbitals, which result in stronger London dispersion forces between molecules compared to the commonly used aromatic capping agents like naphthalene or Fmoc motif. It is anticipated that functionalizing the simple amino-acids or dipeptides with NI-chromophore would facilitate the self-assembly of the molecules in water. Thus, in this work, we have designed and synthesized two new phospho precursors **NI-Yp** and **NI-FYp** with the covalently attached NI core at N-terminus for studying the EISA based hydrogelation process. The synthetic procedure for the preparation of new **NI** compounds and the complete characterization data are provided in supporting information. We also synthesized the **Fmoc-Yp** and **Fmoc-FYp** based on the literature protocol for comparing the hydrogelation ability with NI materials.^{13,14} The chemical structures of various Fmoc and NI building blocks are depicted in Figure 1. The EISA process was examined for four different phosphate compounds and the results are shown in Table 1 and Figure S1.

Table 1. Physical properties of amino acid and peptide amphiphiles under various conditions

S.No	Precursor	Gelator	cLog P ^[a] value of gelator	ALP (Unit) ^[b]	Result	Morphology based on TEM
1	Fmoc-Yp	Fmoc-Y	4.2	50 U	Hydrogel	Nanofibers
2	NI-Yp	NI-Y	2.8	50-200 U	Precipitate	Amorphous particles
3	Fmoc-FYp	Fmoc-FY	5.4	50 U	Hydrogel	Nanofibers
4	NI-FYp	-	-	-	Micelles	Spherical nanoparticles
5	NI-FYp	NI-FY	4.0	50 U	Hydrogel	Partially unzipped nanotubes ^[c]

[a] The values of cLogP values were calculated with ChemDraw [b] Amount of ALP unit added in 0.2 mL of the peptide solution dissolved in Tris-buffer at 1 wt%. [c] Sheet type morphological features has also been noticed (see supporting information)

Self-assembly of amino acid-based compounds:

We begin our study to the self-assembly of **NI-Yp** material. The newly designed **NI-Yp** system containing hydrophilic O-phosphate side chain and carboxylic acid group and the hydrophobic NI chromophore. Hydrophobicity is among the factors that influence the self-assembly of the low-molecular weight (LMW) compounds in aqueous condition. The calculated partition coefficient clogP value is the most commonly used measure of hydrophobicity/lipophilicity. The cLogP values of **NI-Yp** and the corresponding dephosphorylated compound **NI-Y** were found to be 1.5 and 2.8 respectively indicating that our **NI-Y** material is hydrophobic in nature. Several examples of low molecular weight hydrogelators (LMWHs) are known in

the literature with the cLogP values ≥ 2.0 .^{34,35} This led us to infer that **NI-Yp** molecules would have hydrogelation ability under EISA mechanism. The results however, go against our hypothesis. Hydrogelation was not obtained for the **NI-Yp** molecule irrespective of the substrate (1-3 wt%) and ALP concentrations (50-200 U). On the other hand, the **Fmoc-Yp** (1 wt%) fragment exhibited pronounced hydrogel formation under EISA condition. The morphology of the enzyme-catalyzed **Fmoc-Yp** and **NI-Yp** samples was determined by transmission electron microscope (TEM). Self-assembly of **Fmoc-Yp** in presence of ALP resulted in the formation of nanofibers which is consistent with the literature. The TEM image of the **Fmoc-Y** hydrogelator revealed a highly entangled and long continuous nanofiber network, with average diameters of 12.6 ± 1.6 nm.³⁶ However, **NI-Y** molecule exhibited non-specific aggregates under the similar catalytic condition (Figures 2a and 2b). We acknowledge that **NI-Y** will produce hydrogelation at high acidic pH, but neutral or basic pH seems to be the most suitable condition for ALP catalytic hydrogelation process. These findings lead us to conclude that “hydrogelation propensity” is not confined to a single hydrophobic effect, at least in the case of simple amino acids.

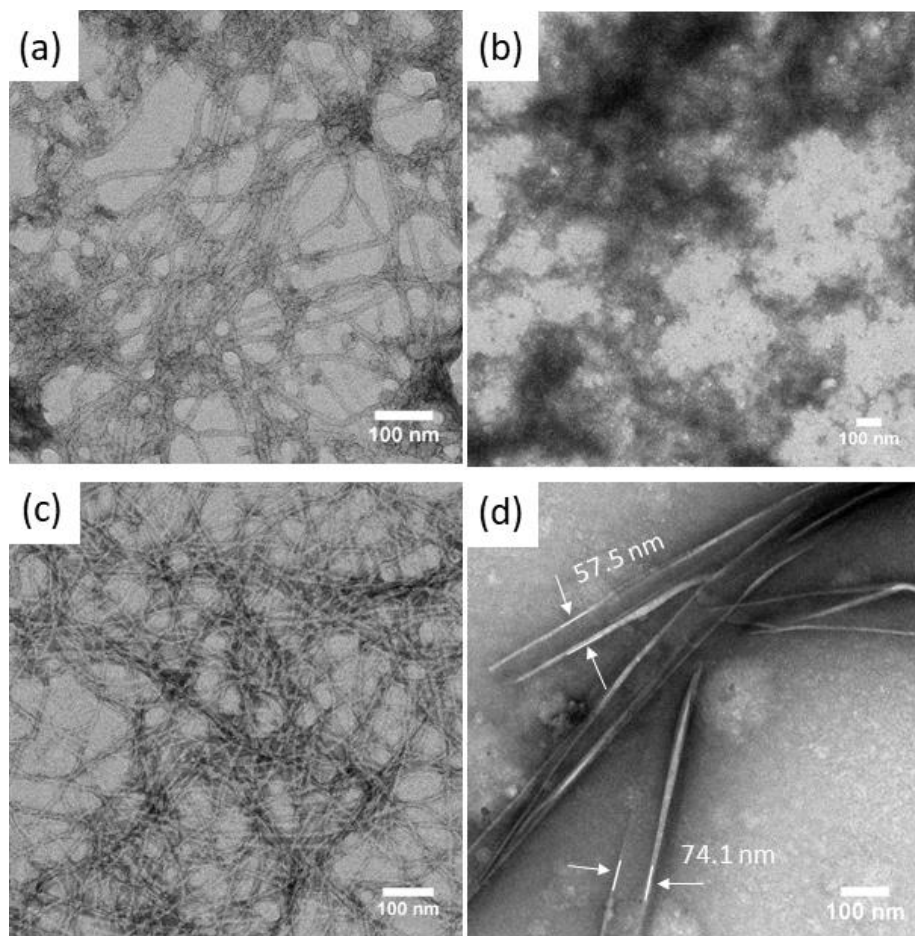


Figure 2. Negatively stained TEM images of ALP treated (a) **Fmoc-Yp**, (b) **NI-Yp**, (c) **Fmoc-FYp** and (d) **NI-FYp**.

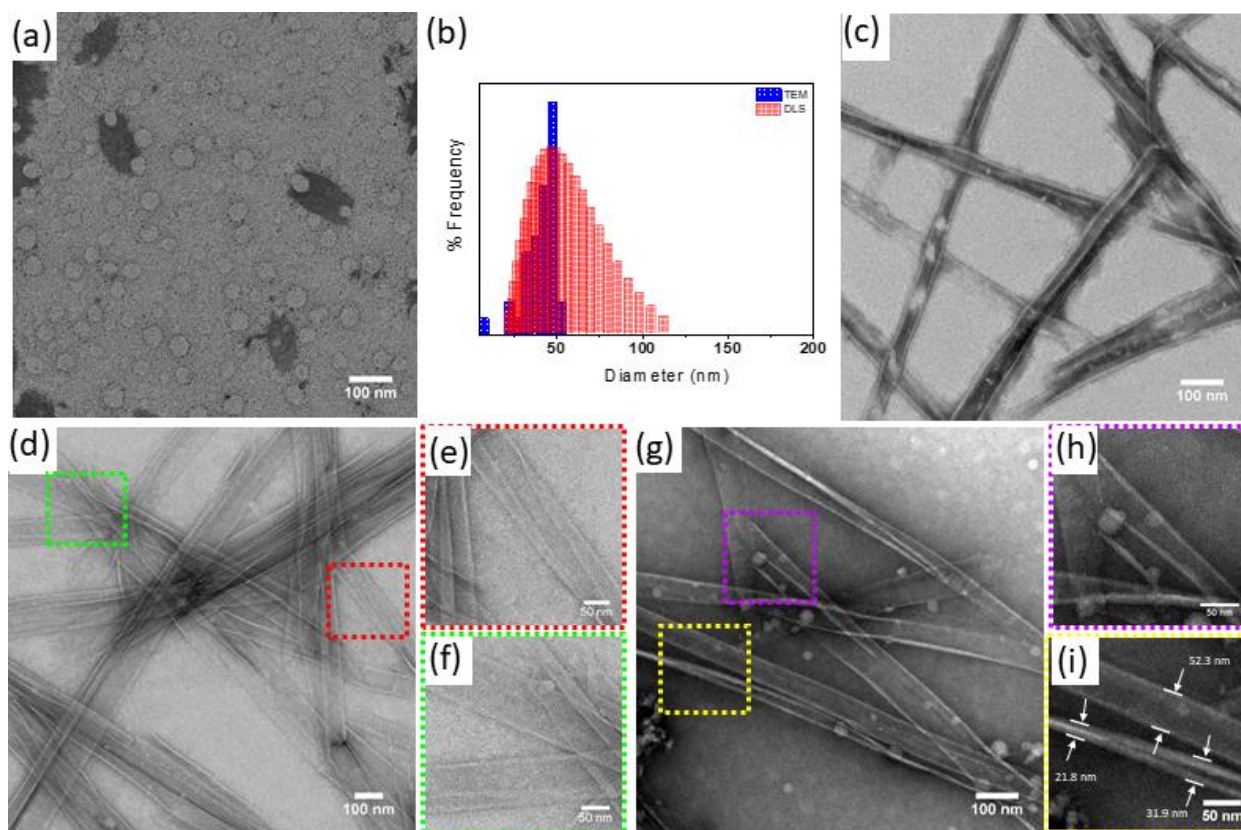


Figure 3. EISA based self-assembly of **NI-FYp** (1 wt%, at 37 °C) in Tris buffer. (a) TEM image of **NI-FYp** nanoparticles in Tris-buffer (10 mM). (b) Particle size distribution histogram of **NI-FYp** (10 mM) nanoparticles by TEM and DLS measurements. TEM images of (c) **NI-FYp** treated with 10 U of ALP (d-f) **NI-FYp** with 20 U of ALP and (g-i) **NI-FYp** with 40 U of ALP.

Self-assembly of dipeptide-based compounds:

Next, we set out to investigate the EISA process for dipeptide hydrogelator. Again **Fmoc-FYp** is the smallest dipeptide core established for EISA process, we prepared a similar dipeptide molecule with NI based N-capping agent. The

calculated cLogP values of **Fmoc-FY** and **NI-FY** were 5.4 and 4.0 respectively. Both the molecules resulted in stable hydrogel under the ALP condition. Self-assembly of **Fmoc-FY_p** resulted in the formation of nanofibers which is consistent with the literature (Figure 2c).³⁷ The TEM image of the hydrogelator **Fmoc-FY** hydrogelator revealed a highly entangled and long continuous nanofiber network, with average diameters of 7.0 ± 0.9 nm. The TEM image of enzymatically dephosphorylated **NI-FY** exhibited nanotubular morphology under the ALP condition (Figures 2d and S3). More interestingly, the width of the nanotubular structure is extended to about 75 nm.

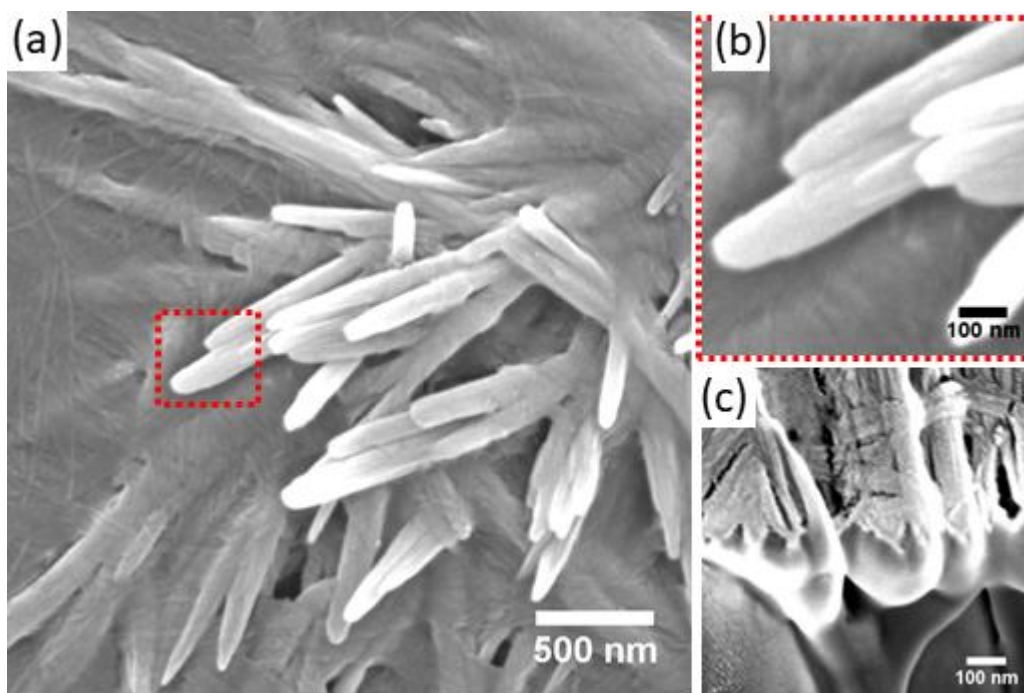


Figure 4. EISA based self-assembly of **NI-FY_p** (1 wt%, at 37 °C) in Tris buffer. (a-b) SEM images of **NI-FY_p** sample treated with 20 U of ALP and (c) SEM cross-section image of FIB milled nanotubular structure.

Supramolecular hydrogels of many reported peptide molecules self-assembled into nanofibrillar morphology with the smallest possible width size, which is much less than 50 nm.²⁷ Few examples of higher-order self-assembled aggregates are also known in the literature.^{19,38,39} Understanding the self-assembly mechanism for the formation of such large aggregates is of significant importance but remains challenging. In this work, we conducted a systematic investigation of the **NI-FYp** system to elucidate the possible mechanism of nanotubular formation. We have done a series of TEM analyses for various samples and the results are summarized in Figure 3 and Table S1. **NI-FYp** at 10mM concentration in water displayed spherical particles in TEM analysis. Such particles also exhibited Tyndall-effect when the solution was irradiated with red-laser light (Figure S2). The particle size and size distribution were determined with dynamic light scattering (DLS) and the value was found to be 50 nm (Figure 3b). The statistical analysis of TEM data shows that the size of the nanoparticles was 27.1 ± 4.6 nm (Figure 3a). The nanoparticles **NI-FYp** self-assembled into a weak hydrogel or viscous solution in presence of 10 U ALP. Increasing the concentration of ALP from 10 to 20 U resulted in a stable hydrogel which could withstand the vial inversion test. Stable hydrogels have also been produced with the ALP range of 20-50 U. Further increasing the concentration of ALP led to the formation of immediate precipitation. In all cases, the self-assembly was noticed within 20 min after the addition of ALP. TEM data were collected and analyzed for the samples at various concentrations of ALP and the results are summarized in Figure 3. The viscous solution with 10U of ALP forms highly ordered nanosheet

aggregates with average diameters of nm 27.3 ± 6.9 nm. Interesting results were obtained as in the case of the **NI-FY_p** sample with 20 and 40U of ALP addition. Nanosheet type structures were obtained as the major morphological feature for the **NI-FY_p** (1 wt%) in aqueous tris-buffer. In some portions of the TEM grid the nanosheets were grooved/curved inwards and rolled-up to form nanotubes. The coexistence of a few twisted nanofibers was also observed with all these conditions (see ESI). Evidently, as depicted in TEM micrographs, these nanostructures are largely entangled, leading to the formation of self-supporting hydrogel networks. In the case of 100U ALP addition, spherical particles were predominantly observed (Figure S5). As we previously described the hydrogels of **NI-FY** at pH 7.0 exhibited nanofibrillar morphological features.²⁹ However, the EISA based self-assembly generated nanotubular peptide assembly. To understand this self-assembly behavior, we have done a series of experiments with **NI-FY** under various pH conditions. The concentration-dependent self-assembly behavior of **NI-FY** was examined and the results are shown in figure S6 and S7. Well-defined twisted nano-fibrils were observed at the low peptide concentrations (0.5-1.0 wt%) under neutral pH condition. Increasing the concentration of **NI-FY** resulted in the formation of thicker and rigid nanosheet type structure without any rolled-up morphological features. Further, the higher concentration of peptide (> 2 wt%) destabilizes the gel-phase and accelerates the formation of solid precipitates. The differences in gelation structures are likely due to the influence of salt on the hydrogelation process.⁴⁰ We then characterized the self-assembly of **NI-FY** (1 wt%) at acidic pH value (6.3) and the TEM data

showed the coexistence of nanofibers and nanosheet morphologies (Figure S8). From these results, it is evident that nanosheet structure formation has proceeded through the association of multiple nanofibrils. We propose a similar mechanism for catalytic hydrogelation of **NI-FYp**. However, it is not clear how the large spherical particles formed at the higher ALP concentrations.

NI-FYp samples with lower ALP concentration (20 U) produced highly ordered nanostructures. Samples with 40U and 50 U of ALP showed only minor changes in the morphological features, so we decided to perform further experimental analysis with 20U of ALP. We have recorded the SEM data for the **NI-FYp** (1 wt%) sample treated with ALP (20 U). The SEM data revealed the nanotubular structures formed through the association of multiple nanofibrils which is similar to that of TEM results (Figure 4). Focused Ion Beam Scanning Electron Microscopes (FIB-SEM) technique was used for site-specific milling and imaging of the nanomaterials (Figures 4c and S9). Groove type nanostructures were observed for the self-assembled **NI-FY** peptides which is consistent with the TEM data. The width of the resulting nanostructure is about 100 nm. The findings indicate that the hydrogelation of **NI-FYp** proceed through a hierarchical self-assembly mechanism in which nanofiber formed in the first stage of the self-assembly process. Such fibers served as building blocks for the formation of nanosheet morphology which subsequently rolled-up into nanotubular structures. The self-assembly mechanism of EISA triggered **NI-FYp** molecule is similar to that of the model proposed for the growth of carbon nanotube.⁴¹ However, the NI-dipeptide nanotubes predominantly existed as partially unzipped structures and

the completely matured nanotube formation was not noticed in any experimental conditions. It could be possible that self-assembly of higher peptide analogue would form stable nanotube structures. Further research is needed on NI-based systems to precisely understand such phenomena. We captured the various stages of the self-assembly process with the aid of TEM and SEM and provide conclusive evidences for the molecular mechanism. Nanotube formation is also possible for uncapped diphenylalanine derivatives, but for the N-capped peptide amphiphiles, such mechanism is rare. For example, Gazit et.al proposed a similar mechanism for diphenylalanine molecule and the inter-molecular packing of such molecules is stabilized through strong attractive electrostatic interactions between a free amine and carboxylic acid groups along with the hydrophobic interactions of aromatic side chains.⁴² However, since the **NI-FY** molecule possesses only carboxylic acid, such interactions are less possible. Thus the molecular skeleton of **NI-FY** would have different self-assembling mechanism compare to the diphenylalanine derivatives. Overall, the findings indicate that the EISA based self-assembly of **NI-FY_p** molecule proceeds through a hierarchal mechanism with the formation of tubular structures (Figure 5).

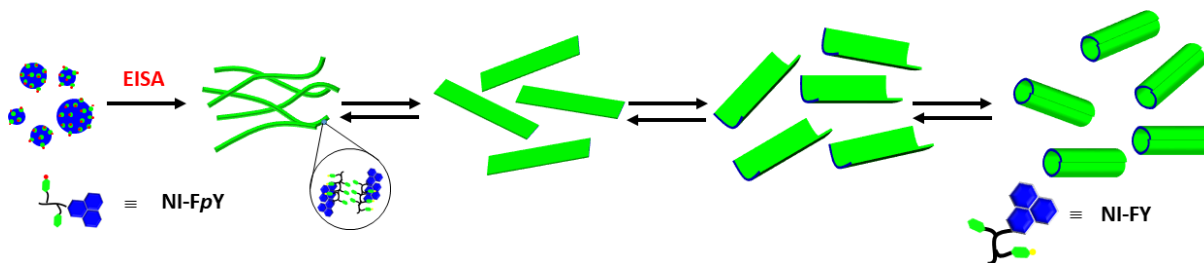


Figure 5. The proposed model for the formation of nanotubular structures that induces hydrogelation.

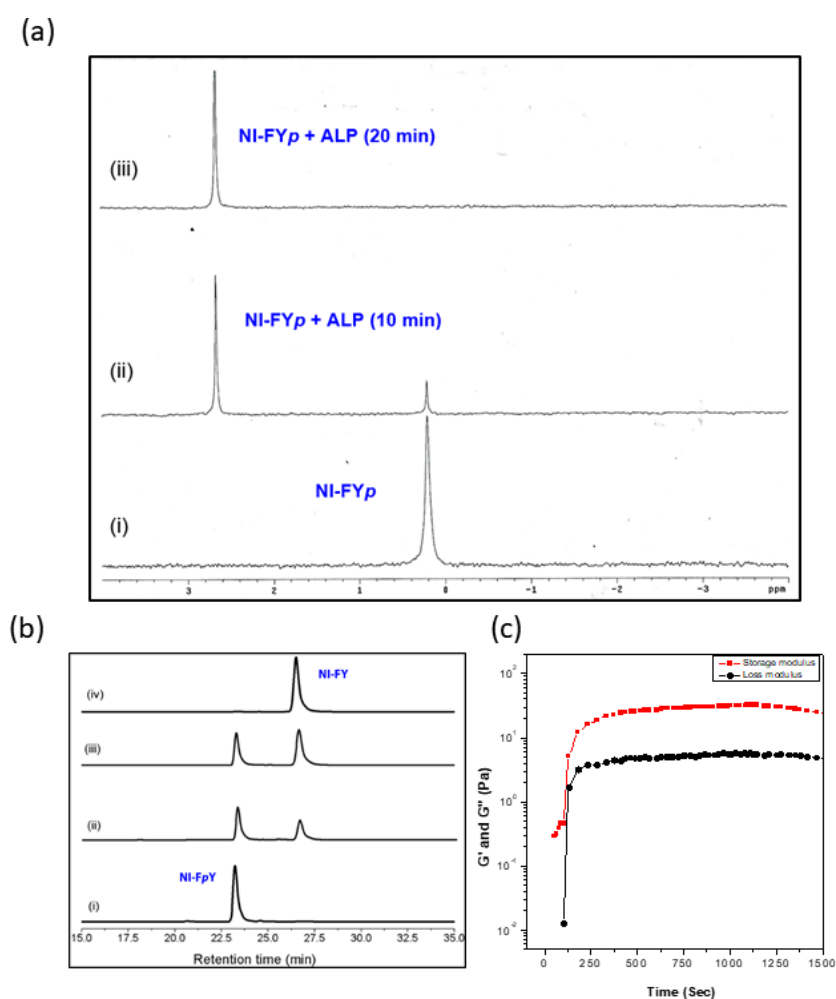


Figure 6. (a) ^{31}P -NMR spectra (in D_2O solvent) for following the EISA based self-assembly of **NI-FYp** sample (1 wt%) (i) without ALP, (ii) with 20 U of ALP measured at 5

min and (iii) 20 min respectively. (b) HPLC profile for monitoring the ALP catalysis of **NI-FYp** at different time interval i) without ALP, (ii) with 20 U of ALP measured at 5 min (iii) 10 min and (iv) 15 min respectively. (c) Time-sweep rheological data of NI-FYp treated with 20 U of ALP for the measurement of gelling point (GP).

Gelation kinetics and rheological studies:

To gain insight into the kinetics of the biocatalytic hydrogelation process we conducted a series of experiments. The hydrogelation process was monitored by ^{31}P -NMR spectra and the data is presented in Figure 6a. The singlet peak at 0.21 ppm is attributed to the signal of **NI-FYp**. For the NMR analysis, the **NI-FYp** sample (1 wt%, 50mM Tris in D_2O) was subjected to the catalytic reaction with ALP (20U). As a result of dephosphorylation, a new peak for the naked phosphate by-product was noticed at 2.66 ppm. The signal intensity of **NI-FYp** decreases with the time and major conversion of **NI-FYp** to **NI-FY** was noticed within 20 minutes of the reaction time suggesting rapid dephosphorylation process. To further examine the enzymatic catalysis process, we decided to use High-performance liquid chromatography (HPLC) and the results are shown in Figure 6b. The HPLC trace exhibited a signal for **NI-FYp** phosphate precursor at retention time (R_t) of 23.2 min. Catalytic dephosphorylation of **NI-FYp** (1 wt%) with 20U of ALP resulted in a new signal at R_t value of 26.5 min confirming the formation of **NI-FY**. The ALP-catalyzed dephosphorylation reaction was completed within 15 min. Such fast hydrogelation kinetics might provide higher rigidity to hydrogel samples through the formation of dense cross-linking networks of the nanostructures.⁴³ We also carried out the

rheological analysis to understand the mechanical stability and gelation kinetics of the **NI-FYp** material in the presence of ALP. Dynamic frequency sweep and time sweep rheological data were measured and the results are shown in Figures 6c and S10. The storage modulus G' (elastic response) and loss modulus G'' (viscous behavior) of the **NI-FYp** sample (treated with 20 U ALP) are independent over the entire frequency range of 0.1-100 Hz which indicate that the hydrogel is viscoelastic in nature. The average G' of the hydrogel at 1 wt% was found to be 97 Pa. The time-dependent rheological data exhibited very low complex modulus initially and the value quickly increased to more than 30 Pa within 250 sec indicating the self-assembly and gelling point (GP) of the sample.

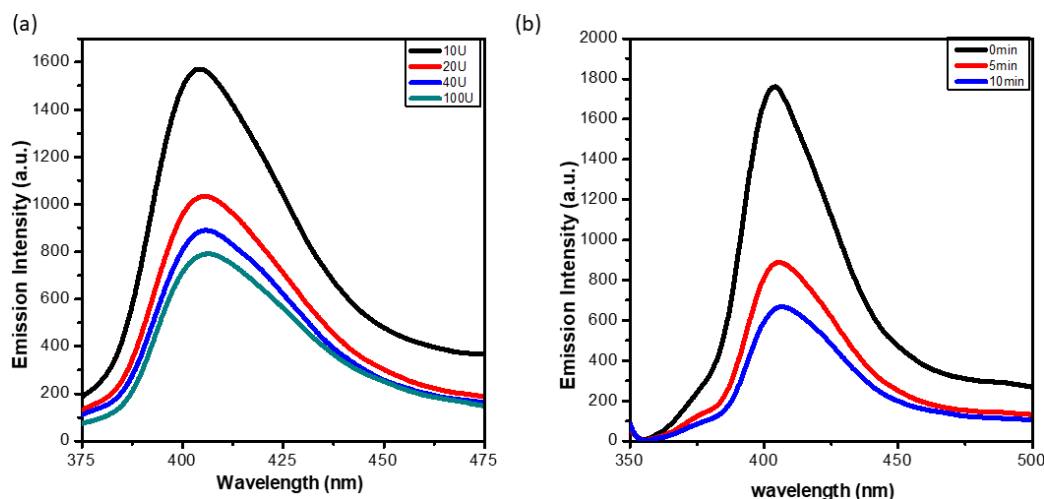


Figure 7. (a) Emission spectra of **NI-FYp** treated with various unit of ALP and (b) Time dependent emission spectra of **NI-FYp** treated with 20 U of ALP.

To understand the supramolecular interactions that are responsible for the self-assembly and hydrogelation process, a series of fluorescence emission spectra

was measured with the excitation at 340 nm (Figure 7 and S11). The emission spectra of **NI-FYp** molecule (1 wt%) in the presence of 20U of ALP showed the fluorescence intensity change in the naphthalimide environment upon the transformation from nanosphere to nanotubular structures. The significant decrease of PL intensity was noticed with the higher concentration of ALP indicating the self-assembly of NI-dipeptide. Time-dependent emission study of **NI-FYp** sample (1 wt%) with ALP (20U) also showed the change in NI emission intensity indicating the aggregation of NI-chromophore. Overall, the results indicating spontaneous self-assembly and hydrogelation of NI-dipeptide.

Spectroscopic and mechanistic studies:

To gain more insights into the intermolecular interactions that are responsible for the self-assembly and hydrogelation process, we carried out UV-Vis absorption, and fluorescence emission measurements.²⁸ Compound **NI-FY** exhibited a strong absorption band at around 340 nm which can be attributed to the electronic transition of NI chromophore (Figure S11). Emission spectra of the **NI-FY** dipeptide in aqueous buffer is shown in Figure 8. The concentration-dependent emission spectra of **NI-FY** were measured with the excitation at 340 nm. The emission signals of **NI-FY** appeared as two peaks at 381 and 394 nm respectively. The emission maximum of **NI-FY** was slightly red-shifted about 6 nm at a higher concentration which is probably due to the presence of strong aromatic interactions. Besides we also carried out the aggregation

study of **NI-FY** in DMSO:water mixture and the results are summarized in in Figures 8b and 8c. To explore whether hydrogelator **NI-FY** has AIE or AIEE characteristics in the assemblies, the PL spectra of **NI-FY** (at 500 μM) were measured in DMSO solvent with different volume fractions of water (f_w). Note that **NI-FY** was completely dissolved and weakly luminescent in DMSO solvent. The emission is intensified with the gradual addition of water into DMSO. When the water fraction $f_w \geq 60$ vol%, a strong blue emission was visually observed under UV irradiation. Upon aggregation at $f_w = 80$ vol%, the **NI-FY** molecule showed a 5.9-fold fluorescent enhancement when compared to that in DMSO. All these results indicate that aggregation has proceeded through strong aromatic intermolecular interactions with AIE characteristics.

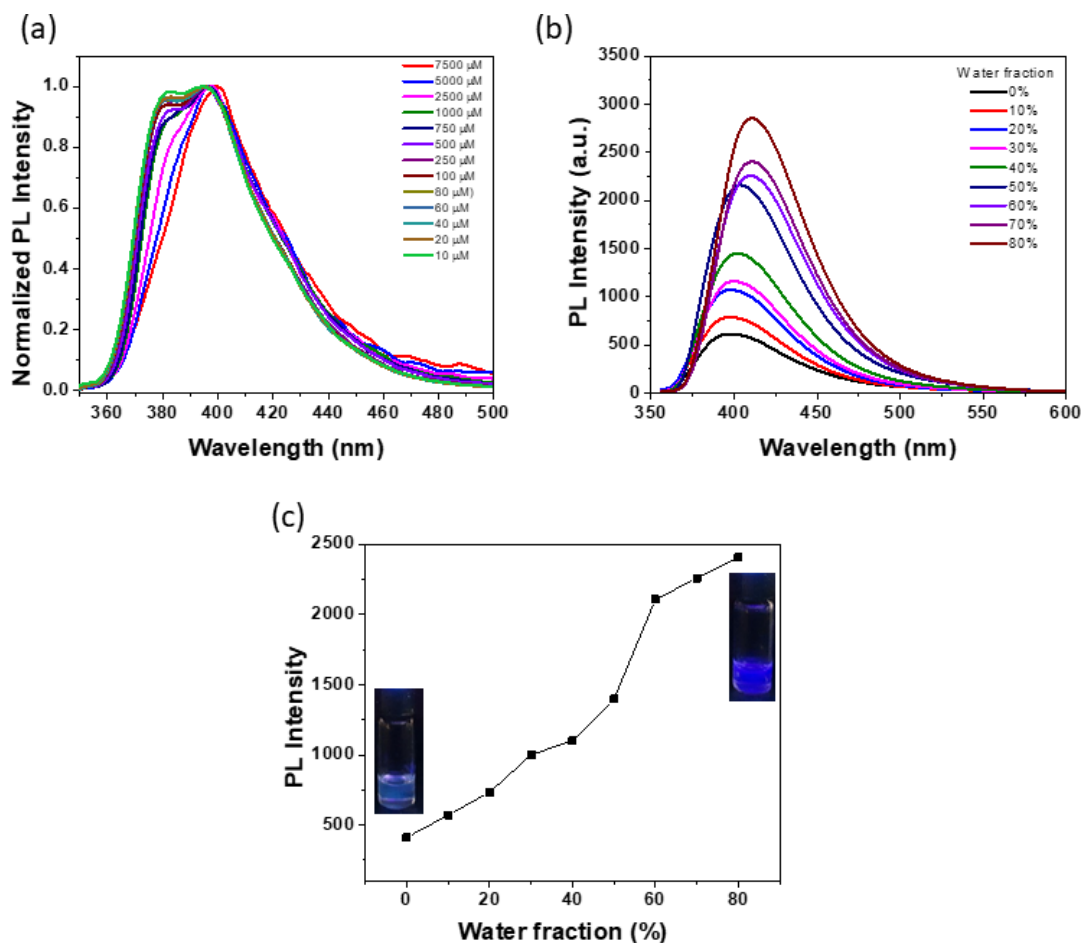


Figure 8. (a) Normalized emission spectra of **NI-FY** at various concentrations in Tris buffer. (b) Emission spectra of **NI-FY** (500 μM) in DMSO:H₂O mixtures with increasing water fractions ($\lambda_{\text{ex}} = 340$ nm) and (c) Plot of emission intensity of **NI-FY** (500 μM) versus the water fractions (fw). The inset of the figure shows the images of **NI-FY** in DMSO-water mixtures with water fraction of 0% and 80 % under UV light.

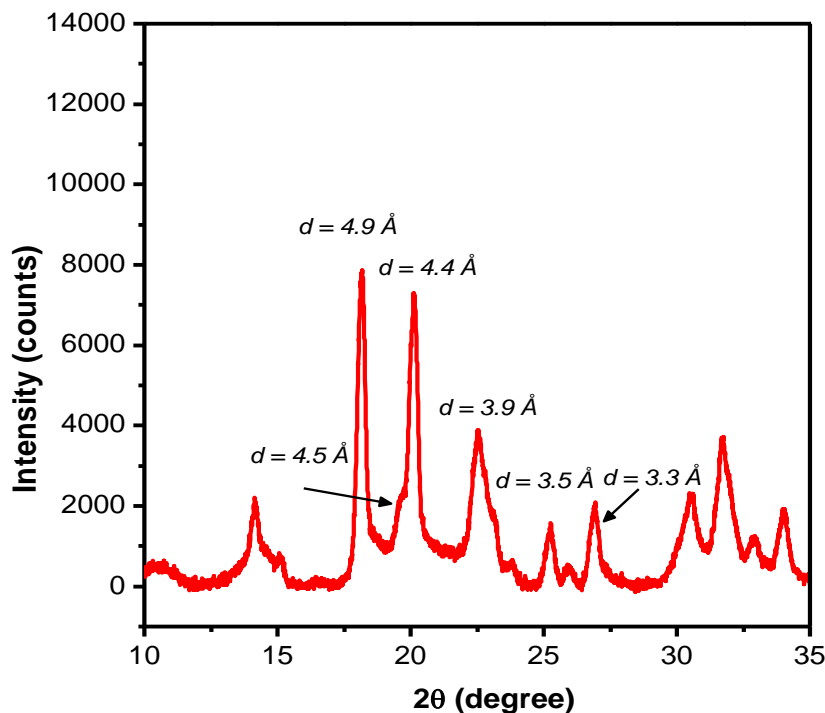


Figure 9. Powder XRD pattern of freeze-dried **NI-FYp** hydrogel with 20U of ALP.

The powder X-ray diffraction (PXRD) pattern of this freeze-dried hydrogel sample showed strong reflections at 4.9, 4.4 and 3.9 Å, indicating the formation of highly ordered structure of the gel samples (Figures 9 and S12). Moreover, the reflections were characteristic of a β -sheet-type structure.^{44,45} A minor reflection at 4.5 Å is most likely due to “cross- β ” type packing orientations.⁴⁶ The reflection at 3.5 Å and 3.3 Å are presumably due to aromatic stacking of NI-core and amino acid side chain.²⁷⁻²⁹ The congo-red staining of **NI-FYp** hydrogel showed apple-green birefringence with polarized light indicating the existence of β -sheet type structures on the hydrogel (Figure S13).

We also used molecular mechanical (MM) calculations with Dreiding Force Field to evaluate noncovalent interactions of the nanostructures of **NI-FY**. We develop an oligomer of ten-molecule model to study the secondary interactions of the basic fibril unit. According to the simulations, the one-dimensional β -sheet-type packing of **NI-FY** is likely to have hydrogen bonding (~ 1.8 Å) and offset aromatic stacking of NI-core with H-centroid distance of around 3.3 Å which is in agreement with the XRD value. (see Figures 10 and S14). The stacking is also stabilized by the hydrogen bonding of the phenolic side chain. These findings conclude that the smallest hydrogel unit is composed of β -sheet-type aggregation along the long axis. During the self-assembly process, two or more such oligomeric units undergo structural transformation stabilized by Phe-Phe interactions and hydrogen bonding, thereby generating matured fibers with a hydrophobic inner core and solvent-exposed carboxyl groups.^{47,48} The matured fibers subsequently self-assembled through solvent-fiber interactions into nanosheet type structures, which further rolled-up into the tubular morphology.

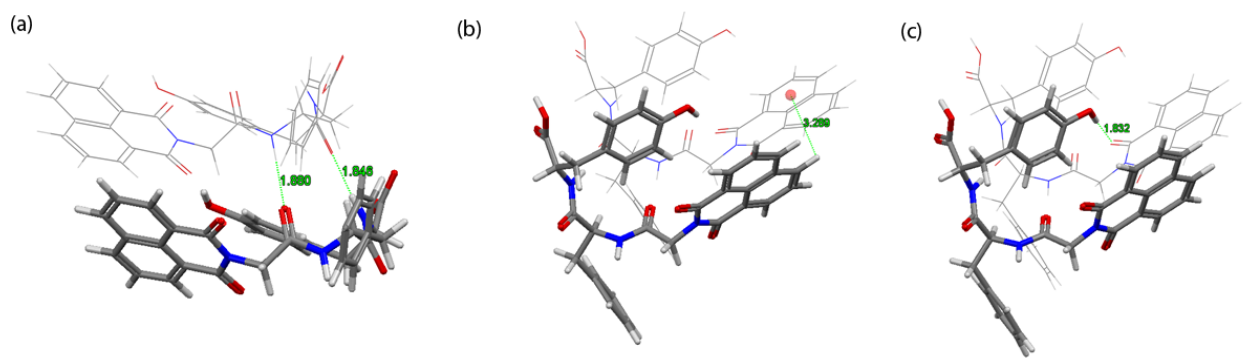


Figure 10. Optimized packing model for **NI-FY** molecules. Possible molecular interactions that are responsible for hydrogelation; (a) Parallel β -Sheet type interactions

via hydrogen bonding of amino-acid backbone (b) Aromatic-stacking of NI core and (c) Hydrogen bonding between phenolic side chain with NI carbonyl group of the neighboring molecule ($O-H\cdots O=C$). Dimer is derived from the optimized one-dimensional packing model of **NI-FY** (see supporting information)

MTT assay for cell toxicity test:

Recently, EISA has been established as a suitable process for selectively killing cancer cells. In order to investigate the cytotoxicity of **NI-FY p** and **Fmoc-FY p** hydrogelators two different types of cancer cell lines were selected; i) human breast cancer cells (MCF7) and ii) human cervical cancer cells (HeLa). The cell viability assay^{49,50} was performed using MTT, the MCF7 and HeLa cells were treated with various concentrations (10 to 200 μ M) of **NI-FY p** and **Fmoc-FY p** over a period of 3 days. The viability rate of MCF7 cells treated with **Fmoc-FY p** was found to be 81% after 3 days' exposure at a high concentration of 200 μ M whereas the percentage of cell viability value of **Fmoc-FY p** treated HeLa cells was decreased to 61.4% at 200 μ M concentration. The **NI-FY p** treated MCF7 cells displayed cell survival ratio over 51.2% at 200 μ M concentration at day 3, In contrast, a large diminution in cell viability was observed with HeLa cells when treated with **NI-FY p** at 200 μ M concentration, only 32.3% cells are viable. Overall, the highest cytotoxic activity was observed with **NI-FY p** (Figure 11). Clearly, the findings indicate that the structure-morphology of the self-assembled material has a significant effect on the cytotoxicity of cancer cells

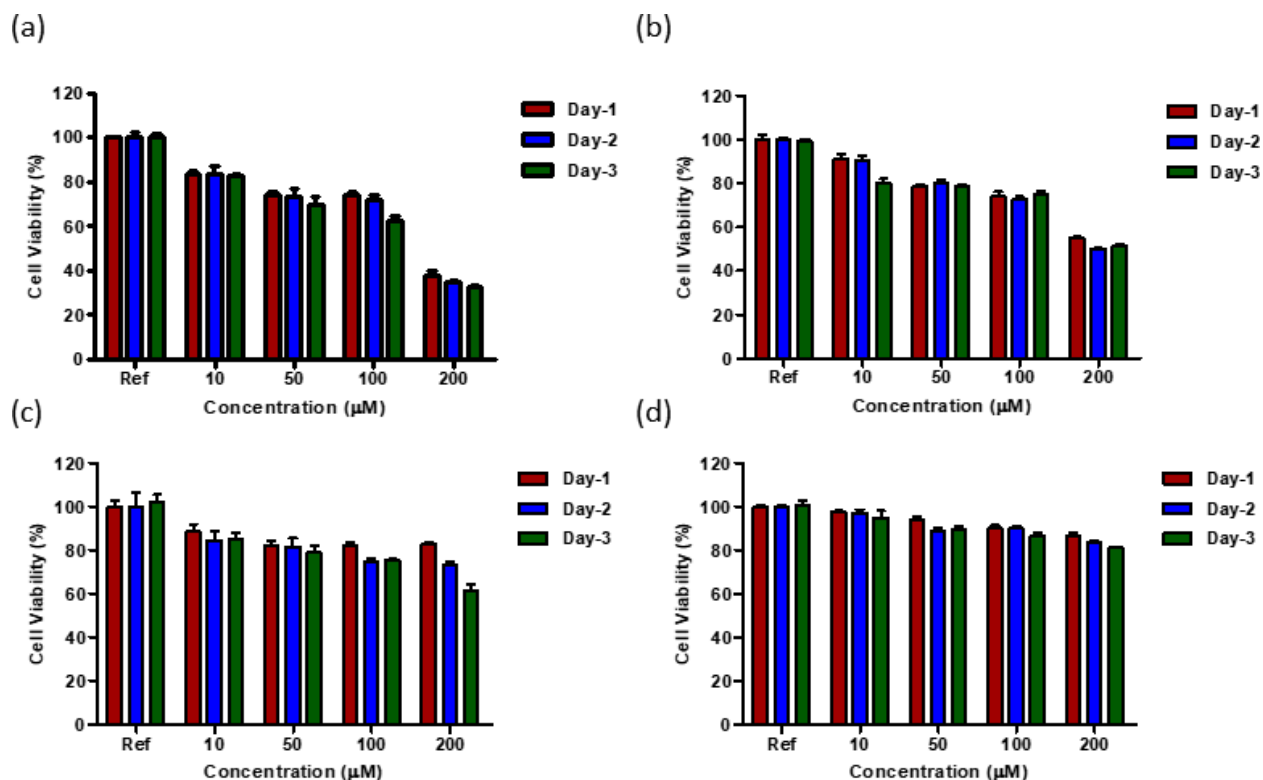


Figure 11. Viability ratios of the HeLa and MCF-7 cells incubated with (a-b) **NI-FYp** and (c-d) **Fmoc-FYp**.

Conclusion

In summary, we have demonstrated the first example of phosphate-based NI/dipeptide conjugate that forms supramolecular hydrogels under the EISA process. The self-assembly of **NI-FYp** has proceeded through multiple stages. The nanofibril structures formed at the initial stage laterally associate to generate nanosheet morphology that further rolled-up into partially unzipped nanotubular structures. The spectroscopic and computational model suggest that the nanostructure of the EISA triggered **NI-FYp** hydrogel is composed of β -sheet-type structure connected by intra- and intermolecular of hydrogen bonding and

aromatic interactions. The phenylalanine side chain provides a possible aromatic interaction for stabilizing the cross- β -structure of the peptide aggregates, but the future research with other NI/dipeptide conjugates is needed to determine the significance of such interactions. The self-assembled nanostructures of **NI-FY** dipeptide have emission characteristics and exhibited higher cytotoxicity to human breast cancer cells (MCF7) and human cervical cancer cells (HeLa), thus making it a potential material for the applications in cancer therapy. We are currently exploring the influences of other parameters that modulate the structures and biological functions of NI-capped hydrogelators.

Acknowledgements

This work was supported by the Ministry of Science and Technology of the Republic of China, Taiwan (MOST grant: 108-2113-M-009-024-).

References

1. G. M. Whitesides, B. Grzybowski, *Science*, **2002**, 295, 2418-2421.
2. Y. Lin, C. Mao, *Front. Mater. Sci.*, **2011**, 5, 247-265.
3. R. Mecham, *The Extracellular Matrix: An Overview*, Springer, Berlin, Heidelberg, 2011.
4. H.-C. Lin and B. Xu, *Applications of Supramolecular Chemistry*, ed. H. J. Schneider, CRC, Boca Raton, FL, 2012, ch. 13
5. M. Zelzer, R. V. Ulijn, *Chem. Soc. Rev.*, **2010**, 39, 3351-3357.
6. N. Singh, M. Kumar, J. F. Miravet, R. V. Ulijn, B. Escuder, *Chem. Eur. J.* **2017**, 23, 981-993.
7. B. B. Gerbelli, S. V. Vassiliades, J. E. U. Rojas, J. N. B. D. Pelin, R. S. N. Mancini, W. S. G. Pereira, A. M. Aguilar, M. Venanzi, F. Cavalieri, F. Giuntini, W. A. Alves, *Macromol. Chem. Phys.*, **2019**, 220, 1900085.
8. M. Konda, B. Kauffmann, D.B. Rasale, A. K. Das *Org. Biomol. Chem.*, **2016**, 14, 4089-4102.

9. M. De Zotti, B. Muzzi, E. Gatto, B. Di Napoli, C. Mazzuca, A. Palleschi, E. Placidi, F. Formaggio, C. Toniolo, M. Venanzi, *J. Phys. Chem. B*, **2018**, *122*, 6305-6313.
10. J. J. Panda, V. S. Chauhan, *Polym. Chem.*, **2014**, *5*, 4418-4436.
11. E. T. Pashuck, S. I. Stupp, *J. Am. Chem. Soc.*, **2010**, *132*, 8819-8821.
12. H. Cui, T. Muraoka, A. G. Cheetham, S. I. Stupp, *Nano Lett.*, **2009**, *9*, 945-951.
13. J. W. Sadownik, J. Leckie, R. V. Ulijn, *Chem. Commun.*, **2011**, *47*, 728-730.
14. K. Thornton, Y. M. Abul-Haija, N. Hodsonc, R. V. Ulijn *Soft Matter*, **2013**, *9*, 9430-9439.
15. W. Wang, Y. Chau, *Soft Matter*, **2009**, *5*, 4893-4898.
16. M. Ueda, A. Makino, T. Imai, J. Sugiyama, S. Kimura, *Chem. Commun.*, **2011**, *47*, 3204-3206.
17. H. Shao, J. R. Parquette, *Angew. Chem. Int. Ed.*, **2009**, *48*, 2525-2528.
18. S. Y. Qin, Y. F. Chu, L. Tao, S. S. Xu, Z. Y. Li, R. X. Zhuo, X. Z. Zhang, *Soft Matter*, **2011**, *7*, 8635-8641.
19. C. Tang, A. M. Smith, R. F. Collins, R. V. Ulijn and A. Saiani, *Langmuir*, **2009**, *25*, 9447-9453.
20. C. Diaferia, G. Morelli and A. Accardo, *J. Mater. Chem. B*, **2019**, *7*, 5142-5155.
21. J. Raeburn, G. Pont, L. Chen, Y. Cesbron, R. Lévy and D. J. Adams, *Soft Matter*, **2012**, *8*, 1168-1174.
22. D. Jacquemin, E. A. Perpète, G. Scalmani, I. Ciofini, C. Peltier, C. Adamo, *Chem. Phys.*, **2010**, *372*, 61-66.
23. S. Huang, R. Han, Q. Zhuang, L. Du, H. Jia, Y. Liu, Y. Liu, *Biosens. Bioelectron.*, **2015**, *71*, 313-321.
24. P. Gopikrishna, N. Meher, P. K. Iyer, *ACS Appl. Mater. Interfaces*, **2018**, *10*, 12081-12111.
25. S. Banerjee, E. B. Veale, C. M. Phelan, S. A. Murphy, G. M. Tocci, L. J. Gillespie, D. O. Frimannsson, J. M. Kelly, T. Gunnlaugsson, *Chem. Soc. Rev.*, **2013**, *42*, 1601-1618.
26. X. Cao, L. Meng, Z. Li, Y. Mao, H. Lan, L. Chen, Y. Fan, T. Yi, *Langmuir*, **2014**, *30*, 11753-11760.
27. S.-M. Hsu, F.-Y. Wu, H. Cheng, Y.-T. Huang, Y.-R. Hsieh, D. T.-H. Tseng, M.-Y. Yeh, S.-C. Hung, H.-C. Lin, *Adv. Healthcare Mater.*, **2016**, *5*, 2406-2412.
28. M. Y. Yeh, C. T. Huang, T. S. Lai, F. Y. Chen, N. T. Chu, D. T. H. Tseng, S. C. Hung, H. C. Lin, *Langmuir*, **2016**, *32*, 7630-7638.
29. S.-M. Hsu, R. D. Chakravarthy, H. Cheng, F.-Y. Wu, T.-S. Lai, H.-C. Lin, *New J. Chem.*, **2018**, *42*, 4443-4449.
30. J. Zhou, X. W. Du, N. Yamagata, B. Xu, *J. Am. Chem. Soc.*, **2016**, *138*, 3813-3823.

31. Z. Yang, G. Liang, B. Xu, *Acc. Chem. Res.*, **2008**, *41*, 315-326.
32. Q. Yao, Z. Huang, D. Liu, J. Chen, Y. Gao, *Adv. Mater.*, **2019**, *31*, e1804814.
33. J. Zhou, X. Du, C. Berciu, H. He, J. Shi, D. Nicastro, B. Xu, *Chem.*, **2016**, *1*, 246-263.
34. L. S. Birchall, S. Roy, V. Jayawarna, M. Hughes, E. Irvine, G. T. Okorogheye, N. Saudi, E. De Santis, T. Tuttle, A. A. Edwards, R. V. Ulijn, *Chem. Sci.*, **2011**, *2*, 1349-1355.
35. C. A. Angulo-Pachón, S. Díaz-Oltra, J. J. Ojeda-Flores, E. Falomir, F. Galindo, J. F. Miravet, *ChemNanoMat*, **2018**, *4*, 769-771.
36. Z. Yang, H. Gu, D. Fu, P. Gao, J. K. Lam, B. Xu, *Adv. Mater.*, **2004**, *16*, 1440-1444.
37. J. K. Sahoo, S. Roy, N. Javid, K. Duncan, L. Aitken, R. V. Ulijn, *Nanoscale*, **2017**, *9*, 12330-12334.
38. Y. Lin, M. Penna, M. R. Thomas, J. P. Wojciechowski, V. Leonardo, Y. Wang, E. T. Pashuck, I. Yarovsky and M. M. Stevens, *ACS Nano*, **2019**, *13*, 1900-1909.
39. W. Liyanage, W. W. Brennessel and B. L. Nilsson, *Langmuir*, **2015**, *31*, 9933-9942.
40. S. Roy, N. Javid, J. Sefcik, P. J. Halling and R. V. Ulijn, *Langmuir*, **2012**, *28*, 16664-16670.
41. C. Gao, Z. Guo, J.-H. Liu, X.-J. Huang, *Nanoscale*, **2012**, *4*, 1948-1963.
42. E. Gazit, *Chem. Soc. Rev.*, **2007**, *36*, 1263-1269.
43. C. X. Chen, Y. F. Gu, L. Deng, S. Y. Han, X. Sun, Y. C. Chen, J. R. Lu, H. Xu, *ACS Appl. Mater. Interfaces*, **2014**, *6*, 14360-14368.
44. O. Rathore, D. Y. Sogah, *J. Am. Chem. Soc.*, **2001**, *123*, 5231-5239.
45. M. Sunde, L. C. Serpell, M. Bartlam, P. E. Fraser, M. B. Pepys, C. C. F. Blake, *J. Mol. Biol.*, **1997**, *273*, 729-739.
46. H. Shao, T. Nguyen, N. C. Romano, D. A. Modarelli and J. R. Parquette, *J. Am. Chem. Soc.*, **2009**, *131*, 16374-16376.
47. J. K. Wychowanec, M. Iliut, M. Zhou, J. Moffat, M. A. Elsayy, W. A. Pinheiro, J. A. Hoyland, A. F. Miller, A. Vijayaraghavan and A. Saiani, *Biomacromolecules*, **2018**, *19*, 2731-2741.
48. I. Ramos Sasselli, P. J. Halling, R. V. Ulijn and T. Tuttle, *ACS Nano*, **2016**, *10*, 2661-2668
49. K. Reichenbacher, H. I. Suss and J. Hulliger, *Chem. Soc. Rev.*, **2005**, *34*, 22.
50. J. L. Guan, *Cell Migration: Developmental Methods and Protocols*, Humana Press, 2005.